## CHEMISTRY

# Natural corrosion-induced gold nanoparticles yield purple color of Alhambra palaces decoration

**Carolina Cardell[1]\*† and Isabel Guerra[2]†**

Despite its fame as a chemically inert noble metal, gold (alloys) may suffer degradation under specific scenarios. Here, we show evidence of electrochemically corroded gilded tin plasterwork in the Alhambra (Granada, Spain) driving spontaneously made gold nanospheres with the optimal size (ca. 70 nm) to impart purple color at the surface. Purple gold on damaged artworks is found sparsely, and its formation is not fully explained yet. We prove that our decayed gold/silver-tin ornament is due to sequential/coexisting galvanic corrosion, differential aeration corrosion, and dealloying of nonperfectly bonded and defect-based metals. Damage is enhanced by exposure to a chloride-rich atmosphere. A white gypsum coat applied during the 19th century to overlap the unaesthetic gilding assists observation of the gold-based purple color. Our work demonstrates gold dissolution, millimetric migration, physical translocation, and deposition as secondary pure gold nanospheres over a centurial time scale under natural environmental conditions.

## INTRODUCTION

Pure gold (Au) is the least reactive metal in natural and industrial environments. Au does not discolor under sunlight or alter under common environmental situations including humidity, air pollution, corrosive gasses, and high temperatures. However, Au (alloys) may undergo dissolution-precipitation, stress corrosion cracking, and tarnishing under particular scenarios (*1–3*), as described in diverse disciplines of science and technology (*3*) including Cultural Heritage Science (*1*, *4*, *5*). With the evolution of metallurgical technologies, the Au quantities required to yield solid objects drove the process of gilding. Gilding is the use of an Au layer to decorate the whole or parts of some other material (*6–9*). Improved gilding techniques emerged when thinner Au layers, i.e., foil (>10 μm width) or leaf (0.1 to 10 μm width), could be achieved as methods to purify Au advanced, and procedures evolved to physically or chemically bond Au to an underlying metal/alloy (*9*). Since an Au leaf cannot support its own mass, artisans have invented many recipes to adhere Au on diverse substrates (*7–9*). The most common gilding processes in artworks are mordant gilding and water gilding. Many others have been adapted from these two basic methods (*7*, *8*). Worthy of mention is gilded tin where a tin (Sn) foil offers the Au leaf a thicker support, assuring easier handling of the composite. Although gilded tin was costlier than gold leaf, it was used because of its higher malleability and thickness.

Cennino Cennini (Italian artist and writer, ca. 1370–1440) shows in his *Libro dell'Arte* how to prepare and use gilded tin on a wall painting where this method is particularly useful (*10*). Gilded tin was common during the Italian Renaissance (*11*). Less known is that it was used to decorate the plasterwork of walls and *muqarnas* (stalactite-type ornaments) in the medieval Muslim Alhambra monument (Fig. 1A) (*12*, *13*). Cardell-Fernández and Navarrete-Aguilera (*12*) described this gilding method in the Alhambra palaces and the occurrence of an odd and diffuse purple color on the surface of

severely degraded gilded tin, always in moist areas that for this reason were later covered with a white gypsum coat (Fig. 1, B and C). They found chloride compounds, but no minerals or dyestuffs responsible for the purple color, which they suggested had to be related to metallic weathering. Its origin remained unknown until now, when we applied a high-resolution field-emission scanning electron microscope (HRFESEM) equipped with energy-dispersive x-ray (EDX) spectrometer coupled to a Raman microspectrometer (RM) in a hyphenated system [structural chemical analyzer (SCA)] (*14*), and high-resolution transmission electron microscopy (HRTEM). We thus acquired high-quality compositional analyses and images at the nano- and microscale from intricate and minute bulk gilded samples and their cross sections to reveal that the purple color is due to Au nanoparticles (AuNPs). To our knowledge, purple color due to AuNPs on damaged artworks is only cited in marbles (*15*), and the comprehensive description of the process causing this color has not yet been explained.

Although Au is said to be corrosion free, we know that Au can dissolve in aqua regia (1:3 molar mixture of $HNO_3$ to HCl) and, for instance, in mixture solutions that yield chlorine (Cl) or are NaCl saturated at room temperature (*1*, *2*, *15*, *16*). Certainly, Au can be reactive in diverse conditions provided that a strong oxidant and a complexing ligand for Au cations are present (*1*, *2*, *17*). Historically important is the use of aqua regia to create the pigment Purple of Cassius since the Middle Ages (*4*, *5*, *18*). Aqua regia holds the oxidizing and complexing agents to dissolve Au. This way, $[AuCl_4]^-$ complexes are formed and, once exposed to a $SnCl_2$ solution, result in AuNPs because $Sn^{2+}$ reduces $Au^{3+}$ to $Au^0$ (*5*). The use of AuNPs for coloring glass, however, was known since antiquity (*19*, *20*). The archives of Ashurbanipal (6400 BCE) in Ninive describe how to impart glass with a violet color using Au particles (*15*). AuNPs were also used in the Roman (4th century CE) Lycurgus glass cup, which displays red or green color when illuminated with either transmitted or reflected light, respectively (*21*). However, the nature of the ruby/violet gold was not unraveled until 1856 when Michael Faraday stated that the gold particles must be very tiny and the color arose from a light scattering effect. Light extinction by AuNPs produces colors ranging from reds to purples and blues and, finally, to brown, depending on particle size, shape, structure, and aggregation state

[1]Department of Mineralogy and Petrology, Faculty of Science, University of Granada, Av. Fuentenueva S/N, 18071 Granada, Spain. [2]Scientific Instrumentation Centre, University of Granada, Campus Universitario Fuentenueva, 18071 Granada, Spain.
\*Corresponding author. Email: cardell@ugr.es
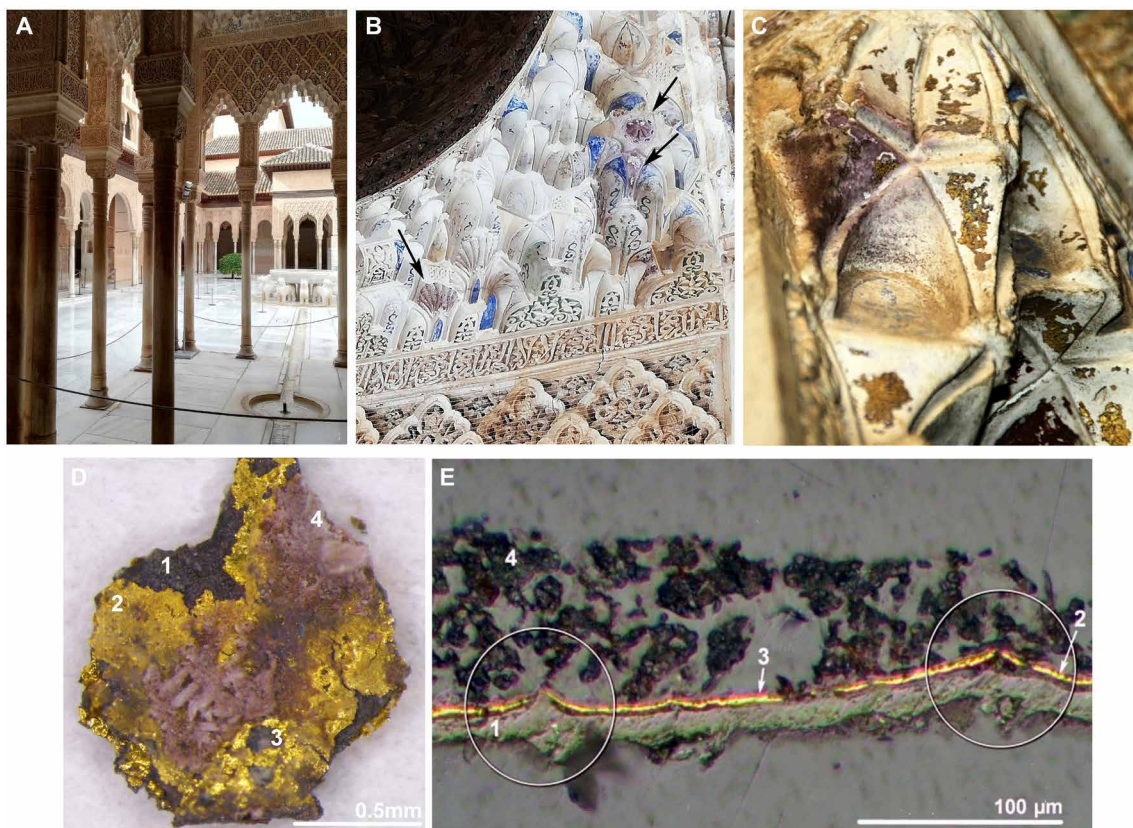†These authors contributed equally to this work.

**Fig. 1. Gilded tin on plasterwork at the Alhambra palaces.** (**A**) General view of the Lions palace. (**B**) Polychrome remains exhibiting traces of purple color at confined wet sites (black arrows). (**C**) Damaged gilded tin with areas tinted purple in the *muqarnas*. (**D**) SM image of the gilded tin structure showing from inside to outside: corroded gray-black metallic foil (layer 1); damaged metallic golden leaf (layer 2); fragments of iridescent purple-grayish covering (layer 3); and purple-tinted whitish coat at surface (layer 4). (**E**) PLM image of the gilding cross section (reflected light parallel polars). Note the irregular surface of the gray metallic foil (layer 1) and the crater-shaped voids in the gilded tin (circles). Note also the spongy texture of the surface coat (layer 4). Photo credit: C. Cardell and I. Guerra, University of Granada, Spain.

(*21*–*23*). These colors result from a phenomenon called localized surface plasmon resonance, when the nanoparticle's surface electrons oscillate in resonance with incident light (*17*, *22*, *24*).

Properties of Au change at the nanoscale, as with other metals and materials, and this has driven nanoparticle research (*19*, *22*, *23*). This challenging field of study is full of open questions, including description of previously unidentified AuNP formation mechanisms. Here, we show a solid and elegant model established from an unexpected combination of processes to spontaneously yield AuNPs. Our finding reveals that the dissolution process of the Au/Ag leaf was other than the traditional dissolution in aqua regia, a product absent in the medium. We demonstrate direct evidence of an unusual electrochemical corrosion-based pathway for our gilded tin that has produced Au nanospheres of different sizes, though mostly of ca. 70 nm, to impart purple color. We shed light on the natural Au dissolution, 1-mm scale migration, and AuNP creation at ambient temperature, over half a millennium.

## RESULTS
### Gilded tin plasterwork decoration: Macro and optical microscopy characterization

Damaged gilded tin is found on plasterworks in (semi)-open areas of the Alhambra palaces at runoff/water condensation sites (Fig. 1, B and C, and fig. S1, A and B). Here, most of the gilding is lost and remains show gray-black, golden, or whitish color displaying an odd purple shade (Fig. 1, B and C). Examination with a stereomicroscope (SM) (Fig. 1D) and a polarized light microscope (PLM) (Fig. 1E) of bulk and cross section samples displays the structure and features of the decoration. The sequence of layers, described from interior to surface, is as follows. The gray-black color points to a porous corroded nonuniform metal foil of 10 to 50 μm width (layer 1). The golden color is due to a friable metallic yellow leaf of average thickness 2 μm (layer 2) that contains fissures, flakes, and rough/rounded voids (fig. S1C). Next, as shown by SM, remnants appear as an iridescent metallic purple shiny covering (layer 3) (Fig. 1D), which is seen as a tiny grayish film under PLM (white arrow in Fig. 1E). At the surface, a purple-tinted whitish coat (average thickness, 70 μm) with spongy texture is found (layer 4). It contains white tabular crystals and some reddish and vitreous crystals (Fig. 1D and fig. S1, C and D). The PLM study shows microlumps in the metal contact surface, which indicates that initially the gray foil was not flat (Fig. 1E). Thus, imperfections and crater-shaped voids are created in the golden leaf. Likewise, PLM reveals that neither metal is well bonded, and a middle organic film is often lacking.

### High-resolution microscopy study and chemical analyses
A comprehensive characterization at micro- and nanoscale of the morphology, texture, elemental and molecular composition of the

gilding, and the purple-colored surface coat is obtained by applying HRFESEM-EDX, HRTEM, and RM-SCA on both bulk and cross section samples. Figure 2 (A and B) shows x-ray maps (see also fig. S2, A to H) and a backscattered electron (BSE) image (Fig. 2C and fig. S2I) of the gilded tin and the surface coating, displaying the identified layers and their composition. From inside to outside, the layers are as follows:

1.) The gray-black foil (layer 1) made of oxidize tin (Sn) where minor amounts of Cl are detected. More precisely, a $Sn^{2+}$ compound, i.e., romarchite (SnO), is identified via RM-SCA (fig. S3A), confirming the corrosion of this metal foil.

2.) The irregular golden leaf (layer 2), which consists of Au alloyed with low amounts of Ag [<5 atomic % (at %)] as indicated by EDX analysis (figs. S2, A and C, and S3B). This highly damaged Au leaf shows porous texture, pits, and microflakes (Figs. 1D and 2C).

3.) The iridescent grayish grime (layer 3) exhibiting cauliflower-like morphology (Fig. 2C). EDX analyses reveal that it has similar composition to the corroded Sn foil (layer 1) (figs. S2B and S3, C and D). Its precise nature could not be identified with RM-SCA due to the nanocrystals that comprise this thin grime.

4.) The surface coat (layer 4) is basically made of sulfur (S) and calcium (Ca) (Fig. 2, A and B, and fig. S2, E and F), which correspond to gypsum ($CaSO_4 \cdot 2H_2O$) according to RM-SCA (fig. S3E). Here, minor amounts of silicates are also found, which are assigned, according to EDX analyses, to quartz ($SiO_2$) (figs. S2G and S3F), Na/K-based phyllosilicates (fig. S3G), and K-feldspar (figs. S2H and S3H). AuNPs appear randomly embedded in this whitish coat (Fig. 2), although they accumulate mainly on the surface of silicate crystals (Fig. 2B and fig. S3H).

High-resolution analyses of the gilded tin using FESEM show frequent crater-shaped voids up to 50 μm in this metal sandwich structure (Fig. 3A). In voids, the Au leaf is worn away exposing the Sn foil (Fig. 3, A and B, and fig. S4). The severely degraded Sn foil displays cracked mud-type microtexture at the surface, and spongy bone type in cross section, which causes its width to increase (Fig. 3, C and D). Corrosion compounds of the Sn foil crept on the Au leaf via these channels (Fig. 3B and fig. S4) forming the porous discontinuous cauliflower-like grime (Fig. 3D and fig. S5). According to TEM analyses, it is made of nanocrystals of abhurite ($Sn_{21}Cl_{16}(OH)_{14}O_6$) and hydroromarchite ($Sn_3O_2(OH)_2$) (fig. S6). Sn-based globular nanoparticles cover the highly porous and fissured

grime. The grime embeds copious Au nanoflakes and Au nanospheres (Fig. 3E and fig. S4A).

Regarding the Au leaf, HRFESEM images acquired at 5 kV reveal that each face of the leaf exhibits dissimilar textural characteristics (Fig. 4A). The internal face in contact with the Sn foil shows corrosion features that yield a cobble-like texture made of tabular/subhexagonal crystals (<300 nm) encircled by nanoscale channels (inset in Fig. 4A). On the external face, in contrast, no shaped crystals are seen. This smooth face shows abundant rounded and irregular nano- and microsize pits (up to ca. 2 μm) displaying terraces with curved convex rims (Fig. 4B). Small isolated shallow pits that spread all over the Au leaf surface coexist with deep etch pits in an advanced damage stage (Fig. 4C). Images suggest that copious and larger pits (ca. 5 μm) result from coalescence of smaller ones, finally causing disaggregation of the Au leaf and resulting in microflakes (Fig. 4D and figs. S4B and S7A). Ag-depleted Au nanospheres of varied size emerge and detach from this external face (Fig. 4E). HRTEM results reveal that the spherical nanoparticles are single $Au^0$ crystals occasionally arranged as grape bunch–like forms (fig. S7).

On the other hand, x-ray maps acquired from the external face of the Au leaf disclose isolated spots of Ag matched with Cl (fig. S8, A to C). Please recall that our Au leaf contains <5 at % Ag. Determination of the exact composition of this silver chloride compound with RM-SCA was not possible due to the small crystal size and the tininess of this leaf. However, EDX analysis suggests that it most likely is chlorargyrite (AgCl) since the ratio Ag:Cl is 1:1 (fig. S8D). As to the surface whitish coat, it consists largely of non-interlocked crystal aggregates of gypsum showing curved borders and subparallel fissures (Fig. 5A). Here, Au nanospheres of typically <200 nm appear erratically distributed, although as stated before they normally concentrate on silicate surfaces (Figs. 2B and 5B).

## DISCUSSION
### Electrochemical corrosion processes of the gilded tin
Our results show that the purple shades seen on the surface of the gilded tin plasterwork at the Alhambra palaces arise from AuNPs with the right size (ca. 70 nm) to impart purple color (Figs. 1 and 5) (17, 18, 21–24). Thus, the occurrence of AuNPs should be related to the slow deterioration of this gilding over centuries that, because of its unaesthetic look, was covered with a gypsum coat (19th century).
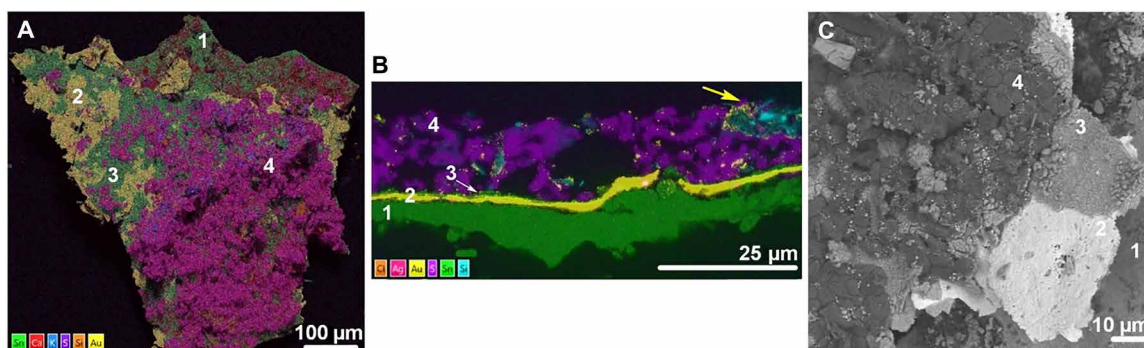
**Fig. 2. Gilded tin structure and composition.** (**A** and **B**) X-ray false color maps showing the gilding layers and their chemical composition. (A) Bulk sample. (B) Cross section sample. (**C**) FESEM-BSE image of the gilded tin. Note the corroded Sn foil (layer 1), the damaged Au leaf (layer 2) with abundant pitting, the grime exhibiting cauliflower-like morphology (layer 3), and the bright AuNPs embedded in the surface gypsum coat (layer 4), mostly located on silicate minerals as displayed in (B) (yellow arrow). Photo credit: C. Cardell and I. Guerra, University of Granada, Spain.
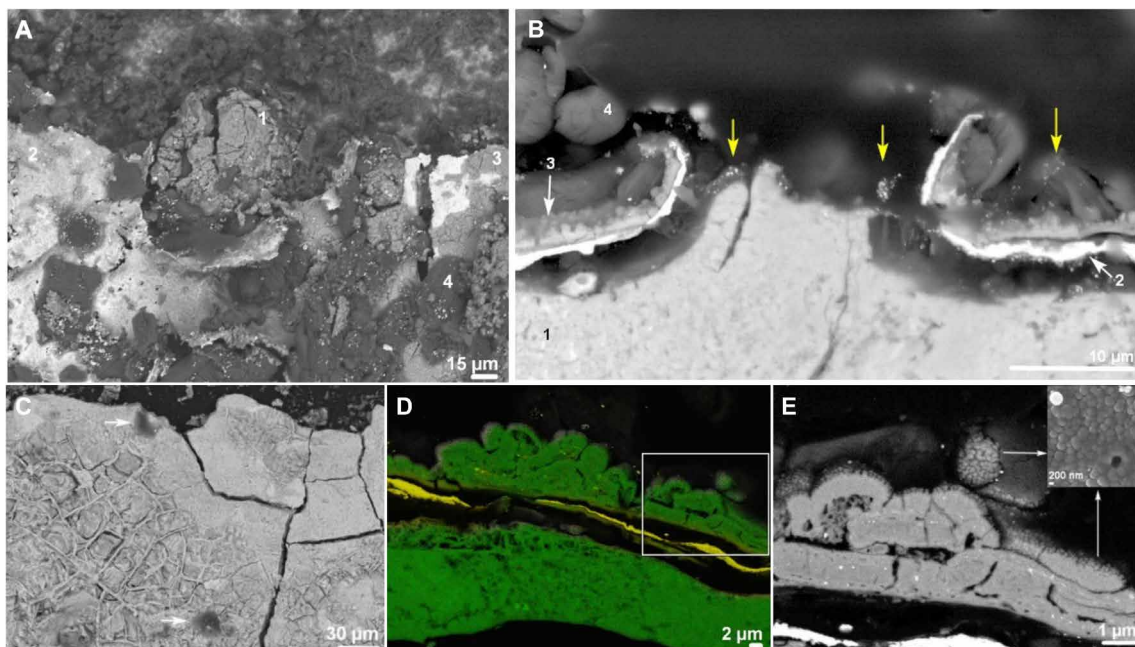
**Fig. 3. FESEM micrographs of damaged gilded tin.** (**A**) BSE image of bulk sample showing a crater-shaped void formed by the Sn foil (layer 1) emerging at the surface through voids of the Au leaf (layer 2). Note that the grime (layer 3) has crept on the Au leaf. Layer 4 is the surface gypsum coat. (**B**) BSE image of cross section displaying the crater-shaped void. Note the porous and fissured Sn foil (layer 1) and the grime (layer 3) above the Au leaf (layer 2). Bright Au nanospheres (yellow arrow) are randomly present. (**C**) SE image of the Sn foil (bulk sample). Note the remains of organic glue (white arrows). (**D**) X-ray false color map showing the spongy texture of the corroded Sn foil (green) and the Sn grime (also green) above the Au leaf (yellow). Note the AuNPs dispersed in the grime. (**E**) BSE image of box in (D) displaying the grime nano-morphology where bright Au nanoflakes and nanospheres are embedded (inset). Photo credit: C. Cardell and I. Guerra, University of Granada, Spain.
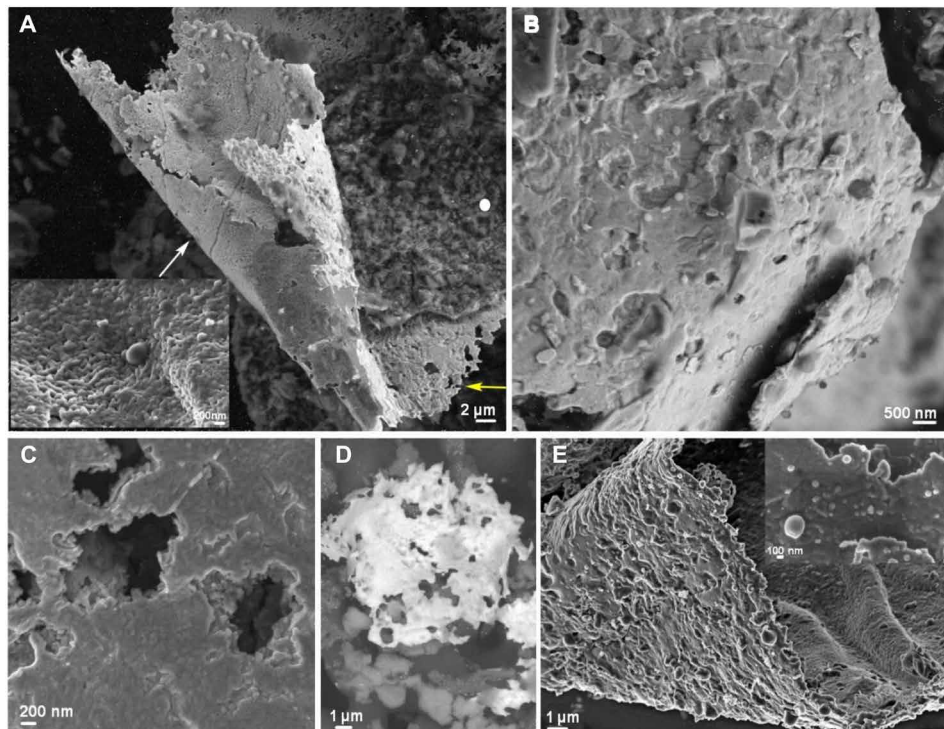


**Fig. 4. FESEM micrographs of the Au leaf (bulk sample).** (**A**) SE image of both sides of the leaf. The internal face (inset, white arrow) shows cobble-like texture. The external face (yellow arrow) exhibits copious pitting and is covered by the grime (white dot). (**B**) SE image of the external face showing varied types (size and profile) of pits. (**C**) SE image of deep etch pits on the external face. Note that tabular crystals of the internal face are seen in their interior. (**D**) Coalescence of pits and subsequent nanoflake formation in the Au leaf (BSE image). (**E**) Distinctive features of the Au external face, i.e., Au nanospheres detaching from the surface coexist with copious pitting. Inset shows a detail of spherical AuNPs of diverse sizes (BSE image). Photo credit: C. Cardell and I. Guerra, University of Granada, Spain.
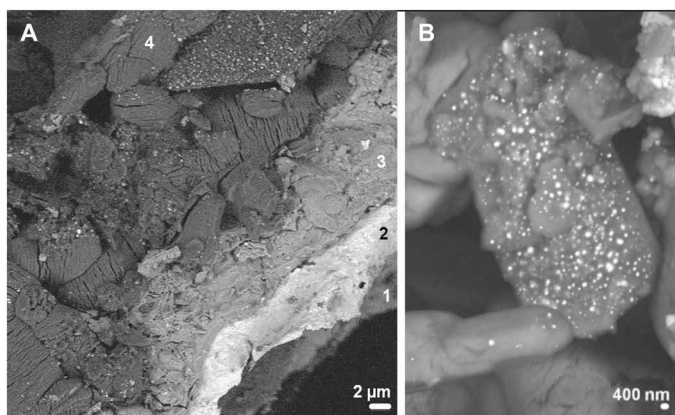
**Fig. 5. FESEM micrographs presenting AuNPs on the surface gypsum coat.** (**A**) BSE image showing gypsum crystals with subparallel fissures (layer 4). Here, bright Au nanospheres are randomly dispersed. Note the underlying grime (layer 3), the Au leaf (layer 2), and the Sn foil (layer 1). (**B**) Detail of Au nanospheres deposited on a silicate crystal found in the gypsum coat. Photo credit: C. Cardell and I. Guerra, University of Granada, Spain.

This white coating has enabled a gold spot test (*25*) to detect the purple AuNPs. The structure of our gilded tin consists of a thin Au leaf glued and burnished on a Sn foil (*12*). The literature reports that the stability of gilded metals (i.e., bimetallic gilding) relies on the width and porosity of the Au leaf and its adhesion on the underlying metal. Hence, the presence of imperfections such as voids or fissures will trigger galvanic corrosion (GC) (*5*, *26*).

As seen by the naked eye, our gilded tin is severely damaged (Fig. 1, C and D). PLM shows that voids and defects in the Au leaf surely formed during its burnishing on the Sn foil (Fig. 1E). Also, adhesion between both metals is deficient due to degradation/loss of the nonconductive intermediate organic film (Fig. 3C), which improves their direct electrical contact. All these features, in the presence of water/moisture and a Cl⁻-rich medium (as clarified below), generate alteration of the gilded tin by GC. During GC, two dissimilar metals/alloys in direct contact corrode differently in an electrolyte solution. GC is a complex process where material, environmental, and (metal/alloy) geometrical factors govern the corrosion extent (*26*, *27*).

Crater-shaped voids and fissures in our thin Au leaf (Figs. 1E and 3, A and B) are channels through which water/moisture reaches the underlying Sn foil. These channels provide an ionic pathway between the two metals promoting microgalvanic cells. Here, Sn (the less noble metal) is the anode and undergoes oxidation by losing electrons according to the anodic reaction Sn (s) → $Sn^{2+}$ + $2e^-$, and thus corrodes. Consequently, electrons move from the Sn toward the Au (the more noble metal). However, Au does not participate in the cathodic reaction. Au acts as an inert electrode (and remains protected) and supports the cathodic reaction, which is oxygen reduction: $O_2$ + $2H_2O$ + $4e^-$ → $4OH^-$ (Fig. 6, A and B). Note that an electrolyte is needed for GC to occur. Moreover, GC aggressivity increases in marine environments, as well as in atmospheres rich in gaseous pollutants (*26*, *27*). Marine aerosols (mainly Cl⁻-rich) are present in the city of Granada and at the Alhambra (*28*). Levels of gaseous and particulate pollutants are also among the highest in Spain (*28*, *29*). High relative humidity at the Alhambra palaces (up to 93% in winter) (*28*) likewise should increase GC rates (*5*, *26*, *27*).
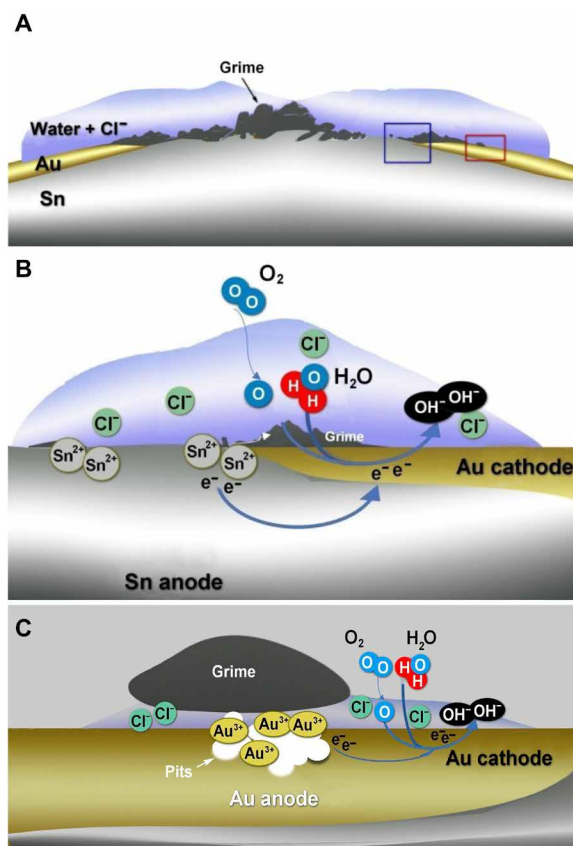


**Fig. 6. Schematic diagrams showing the electrochemical corrosion processes occurring in the gilded tin.** (**A**) General view of the operating corrosion processes. (**B**) Galvanic corrosion of the Sn foil [blue box in (A)]. (**C**) Differential aeration corrosion of the Au leaf [red box in (A)].

In the corroded Sn foil, our FESEM, RM-SCA, and TEM analyses identify $Sn^{2+}$ compounds, while the $Sn^{4+}$ compound, i.e., cassiterite ($SnO_2$), is absent. These results agree with a previous work made in the Alhambra in similar gilding samples (*13*) and with findings in pewter artifacts exposed to sea water conditions (*30*). The cited $Sn^{2+}$ compounds pushed up and crept onto the Au leaf through the voids and deposited as overlying grime, defacing the gilding (Fig. 1, C and D). Note that this GC process is only responsible for the Sn foil damage and does not explain the weathering and dissolution of the Au leaf at its external face (in contact with the grime) (Fig. 4, A and B). Corrosion of this Au external face is caused by its partial coverage with the grime (Figs. 2C and 5) that yields differences in oxygen concentration on its surface. As a result, oxygen concentration cells are created and differential aeration corrosion occurs (corrosion caused by the potential difference of a metal/alloy exposed to dissimilar environments) (*31*). Sites of the Au leaf uncovered by grime are well oxygenated and remain cathodic (so protected), while covered areas have low-oxygen concentration and become the anode (Fig. 6C). Hence, Au anodic dissolution (oxidation/dissolution) occurs in these localized oxygen-deficient (anodic) areas in parallel with pit growth (Fig. 4B) (*31*).

Corrosion of the Au leaf is assisted by its thinness (*32*), roughness (*16*), and Ag content (*5*, *33*). Corrosion is further enhanced by the Cl⁻-rich environment (*27*). Proof of this is the presence at the

external leaf face of chlorargyrite, whose insolubility and immobilization enable its EDX detection. Chlorargyrite formation can be ascribed to Ag oxidation in the $Cl^-$-rich electrolyte, the aqueous-phase reaction followed by precipitation expressed as $Ag^+ + Cl^- = AgCl$ (s). Note that, in agreement with the condition of AgCl formation, Ag oxides are not found here (34). On the other hand, it is known that the resistance of metals to corrosion increases in proportion to reduction potential. Thus, our $Cl^-$-rich solution likewise assists the Au dissolution by diminishing it reduction potential ($E^0$), as shown in the following reduction half-reactions (16): $Au^0$ (s) $\leftrightarrow Au^{3+}$ (aq) $+ 3e^-$ ($E^0$ = 1.50 V) and $Au^0$ (s) $+ 4Cl^-$ (aq) $\leftrightarrow [AuCl_4]^-$ (aq) $+ 3e^-$ ($E^0$ = 1.00 V). Note that the last equation is shown here because $Au^{3+}$ complexes are commonly formed in the presence of $Cl^-$ ions in an oxidizing medium (5, 16), with $[AuCl_4]^-$ as the best case of $Au^{3+}$ complex.

As stated above, etch pit growth occurs in parallel with Au oxidation/dissolution improved by the $Cl^-$-rich solution (Fig. 4B) (27). Subsequently, pits coalesce creating larger holes, weakening and ultimately perforating the Au leaf that becomes more brittle (35). This yields mechanically formed Au microflakes (Fig. 4D and fig. S7A). Concurrently, the new pitting creates extra electrochemical cells that promote further corrosion of the Sn foil. Thus, more Sn corrosion products are formed and migrate through the pits. This is a recurrent corrosion process that finally yields an almost continuous cauliflower-like grime on the Au leaf (fig. S5A).

On the contrary, our FESEM nanostructural study reveals that the Au face in contact with the Sn foil (internal face) shows different dissolution features. Two mechanisms, likely working alongside, would explain its cobble-like texture (Fig. 4A, inset). Regarding one potential model, please recall that we have an Au/Ag leaf and that corrosion of Au-Ag alloys occurs under certain corrosive media (e.g., sea water), commonly beginning with selective dissolution of less noble Ag during anodic corrosion (2, 22, 36, 37). This is due to the difference in electrochemical potential between both metals (1, 5). During this dealloying process, random vacancies are formed and Au undergoes surface diffusion and self-reordering to form Au-rich islands bordered by nanoscale pores/channels (2, 22, 32, 37, 38), as seen in Fig. 4A (inset). On the other hand, in line with the model proposed by Cherevko and co-workers (39), in our aerated oxygen-rich medium, $Au^0$ would suffer oxidation due to O/OH adsorption resulting in passivation of the leaf surface by Au oxide formation. De-passivation would follow due to Au ions and O/OH exchanging places. Then, Au dissolution occurs, creating a roughened surface where microchannels run through the Au crystals.

### Formation of AuNPs and Au mobility
Potential Au reducing agents to precipitate spherical AuNPs are manifold (3, 17, 40, 41). This process is enabled because $Au^{3+}$ is a strong oxidant so that it can be reduced by almost any other metal or metal ion (3, 42, 43). Accordingly, we propose that, in our $Cl^-$-rich medium, $Au^{3+}$ is reduced to $Au^0$ by ubiquitous $Sn^{2+}$ compounds producing Au nanospheres (Fig. 4E) (3, 5, 44). Note that AuNP formation by reducing $Au^{3+}$ with $Sn^{2+}$ in chloride solutions can be obtained in both acidic and alkaline solutions (44). The reactions taking place are redox processes, i.e., $Au^{3+} + 3e^- \rightarrow Au^0$ and $Sn^{2+} \rightarrow Sn^{4+} + 2e^-$, where the overall reaction is $2Au^{3+} + 3Sn^{2+} \rightarrow 2Au^0 + 3Sn^{4+}$. We should note that $SnO_2$ (resulting from hydrolysis and precipitation in the medium), according to reaction $Sn^{4+} + 2H_2O \rightarrow SnO_2 + 4H^+$, is required for stabilizing the AuNPs

(5, 44). However, we have not detected $SnO_2$ anywhere in our gilded tin, as mentioned above. Afterward, the created Ag-depleted Au nanospheres should have translocated vertically through the grime toward the surface ornament, likewise the Au microflakes (Figs. 2B, 3E, and 5 and figs. S7A and S9). This process may be governed by the great porosity of both the grime and the gypsum coat, and the high specific gravity of Au (33).

In addition, the preferential setting of Au nanospheres on the silicates found in the surface coat (Fig. 5B) suggests that Au ions have chemically migrated through the ornament. Diverse silicate minerals (feldspars, phyllosilicates, and mainly quartz) are Au pre-robbing agents that can reduce Au-Cl complexes and deposit $Au^0$ nanospheres on their surfaces (primarily via chemisorption), in both acidic and alkaline chloride media at room temperature (42, 45). These findings are based on experiments and quantum chemistry calculations. A three-step electrochemical mechanism is proposed in the literature to explain the adsorption/reduction of Au on silicate surfaces (42). First, it involves chemical migration of negatively charged Au-Cl complexes to positively charged edges of phyllosilicates (clay minerals) or protonated silanol groups on the silicate surfaces (electrostatic attraction). Next, ligand substitution occurs between the Au complexes and $OH^-$ groups on defect sites of silicate surfaces. Last, Au reduction happens by either silicon radicals or hydrogen at the silicate defect sites (42). This is a condensation method (17) among the many synthesis mechanisms and reducing agents that yield AuNPs of ruby/purple color (3, 5, 17, 40, 46). The famous Purple of Cassius method is only one example of AuNP formation (4, 5).

In closing, the electrochemical oxidation/dissolution of Au is a complex subject usually studied under laboratory conditions using ad hoc equipment, methods, and thermodynamic approaches (16, 39). Conversely, here, we propose a pioneering robust model that sheds light on the degradation of bimetallic artistic gilding, including Au dissolution and AuNP precipitation under natural conditions in a $Cl^-$-rich medium. The model demonstrates an unexpected combination of electrochemical processes to yield purple gold color on the surface of our damaged gilded tin. The white color of the gypsum coat applied on this gilding has enabled detection of the purple AuNPs. To our knowledge, purple color on damaged artworks is cited only in an antique marble sculpture (probably covered by a gold leaf, though not seen presently) and was attributed to naturally induced gold corrosion because of a simple but slow process (15). Purple AuNPs on corroded (bimetallic) gildings are likely more widespread but unnoticed because of the lack of an overlying whitish layer on the ornament to reveal the Au dissolution and precipitation processes (26). Last, our research is done on a real case study of more than five centuries of weathering under natural conditions, limiting our ability to elucidate the exact corrosion model. However, the results shown here will hopefully help experts of ancient gilded objects with the information relevant to corrosion methods and materials of intervention, as well as corrosion prevention.

## MATERIALS AND METHODS
### Materials
Samples ($N$ = 15) of gilded tin plasterwork decoration were collected in diverse areas of the Alhambra palaces. In particular, samples proceed from remains of purple-tinted decayed gilded tin that cover the *muqarnas* of the Court of the Lions' pavilions (Fig. 1, A and B),

the *muqarnas* of the entrance arches and vaults of The Hall of the Kings, and the arches of the two lateral open rooms located in the Court of the Myrtles at both sides of the entry to the Chamber of the Ambassadors (Comares Palace) (fig. S1, A and B). Samples were selected considering the diverse colors observed on the surface of the gilded tin that could indicate varied gilding materials, compositional and textural characteristics, damage processes, and location within the Alhambra palaces.

## Instrumentation and characterization methods

The overall structure, texture, color features, and conservation state of the gilded tin samples were examined using a Nikon SMZ 1000 (Japan) SM equipped for microphotography. Next, samples were divided into two parts and one fragment was embedded in an acrylic resin to obtain a paint stratigraphy, prepared as a polished thin section, to examine the gilded tin cross section by PLM using both transmitted and reflected light with either parallel or cross polars. The PLM (Carl Zeiss Jenapol U instrument, Germany) incorporates a digital camera (Nikon D-7000) to help examination of the gilding structure, texture, mineralogy, and conservation state. Each polished thin section and the corresponding gilded tin bulk sample were analyzed using HRFESEM-EDX spectroscopy coupled to an RM via the SCA interface (Renishaw plc., Gloucestershire, UK). A full description of this instrument and its optimized use to examine historical paintings is given by Guerra and Cardell (*14*). The FESEM (Zeiss Supra 40Vp, Germany) is armed with diverse detectors to deliver different images: a secondary electron (SE) (InLens) detector that produces morphological images, a BSE detector that gives chemical images, and a microanalysis system (Aztec 2.2) to provide elemental analyses by EDX. The EDX detector (50-mm$^2$ silicon drift detector XMAX) allows detection of elements with $Z \geq 4$ (Be) and high count rates. The RM (Renishaw inVia) is fitted with a near-infrared diode 785-nm laser and a Nd:YAG 532-nm laser. The FESEM-SCA allows simultaneous SE imaging and Raman analyses on the same sample and area without the limits that accompany the sequential use of FESEM-EDX and RM.

All samples were mounted on Al stubs with double-sided adhesive C tape and carbon-coated to be studied under high vacuum level ($10^{-6}$ torr). EDX single-point analyses were acquired using 15- to 20-kV beam energy and 10 eV ch$^{-1}$ resolution, and high-resolution topographic images were made by the InLens detector working at 5 kV. High-resolution x-ray maps ($1024 \times 768$ pixels) were obtained from selected areas with 500 frames and a dwell time of 10 ms using 3-nA filament current and 20 eV ch$^{-1}$ resolution over 8 hours. Each Raman spectrum presented in this work shows the setup conditions for its acquisition.

The morphology and composition of particular areas from the grime of the gilded tin were studied at nanoscale with an HRTEM FEI Titan G2 microscope operating at 300 kV. The identification of mineral phases was done by collecting selected-area electron diffraction (SAED) patterns using a 180-nm aperture. Compositional maps of interested areas and single-point analyses were obtained in scanning transmission electron microscopy (STEM) mode using a Super-X EDX detector (FEI). A high-angle annular dark-field (HAADF) detector was used to acquire STEM images of the areas studied by EDX. Point-to-point resolution was 0.08 nm in the TEM mode and 0.2 nm in the STEM mode. Before the HRTEM study, samples were dispersed in ethyl alcohol and deposited on a carbon film–coated Cu grid.

## REFERENCES AND NOTES

1. D. A. Scott, The deterioration of gold alloys and some aspects of their conservation. *Stud. Conserv.* **28**, 194–203 (1983).
2. W. S. Rapson, Tarnish resistance, corrosion and stress corrosion cracking of gold alloys. *Gold Bull.* **29**, 61–69 (1996).
3. H. Renner, G. Schlamp, H. M. Lüschow, P. Tews, J. Rothaut, K. Dermann, A. Knödler, C. Hecht, M. Schott, R. Drieselmann, C. Peter, R. Schiele, Gold, gold alloys, and gold compounds, in *Ullmann's Encyclopedia of Industrial Chemistry* (Wiley, 2012), vol. 17, chap. 1.
4. J. Carbert, Gold-based enamel colours. *Gold Bull.* **13**, 144–150 (1980).
5. L. Selwyn, Corrosion chemistry of gilded silver and copper, in *Gilded Metals. History, Technology and Conservation* (Archetype Publications Ltd., 2000), pp. 21–47.
6. M. F. Guerra, T. Galligaro, Gold cultural heritage objects: A review of studies of provenance and manufacturing technologies. *Meas. Sci. Technol.* **14**, 1527–1537 (2003).
7. I. C. A. Sandu, M. H. de Sá, M. C. Pereira, Ancient gilded art objects from European cultural heritage: A review on different scales of characterization. *Surf. Interface Anal.* **43**, 1134–1151 (2011).
8. D. Gulotta, S. Goidanich, M. Bertoldi, S. Bortolotto, L. Toniolo, Gildings and false gildings of the baroque age: Characterization and conservation problems. *Archaeometry* **54**, 940–954 (2012).
9. E. Darque-Ceretti, M. Aucouturier, Gilding for matter decoration and sublimation. A brief history of the artisanal technical know-how. *Int. J. Conserv. Sci.* **4**, 647–660 (2013).
10. C. Cennini, *El Libro del Arte* (AKAL S.L., 1988).
11. R. Billinge, D. Gordon, The use of gilded tin in Giotto's "Pentecost". *Nat. Gal. Tech. Bull.* **29**, 76–80 (2008).
12. C. Cardell-Fernández, C. Navarrete-Aguilera, Pigment and plasterwork analyses of nasrid polychromed lacework stucco in the Alhambra (Granada, Spain). *Stud. Conserv.* **51**, 161–176 (2006).
13. M. J. De la Torre-López, A. Domínguez-Vidal, M. J. Campos-Suñol, R. Rubio-Domene, U. Schade, M. J. Ayora-Cañada, Gold in the Alhambra: Study of materials, technologies, and decay processes on decorative gilded plasterwork. *J. Raman Spectrosc.* **45**, 1052–1058 (2014).
14. I. Guerra, C. Cardell, Optimizing use of the structural chemical analyser (variable pressure FESEM-EDX Raman spectroscopy) on micro-size complex historical paintings characterization. *J. Microsc.* **260**, 47–61 (2015).
15. H. Piening. Gold to purple. Violet traces on antique marble (2013); www.stiftung-archaeologie.de/Heinrich%20Piening%20Gold%20to%20purple%202014.pdf.
16. J. Chinnaiah, O. Kasian, A. Dekshinamoorthy, S. Vijayaraghavan, K. J. J. Mayrhofer, S. Cherevko, F. Scholz, Tuning the anodic and cathodic dissolution of gold by varying the surface roughness. *ChemElectroChem* **8**, 1524–1530 (2021).
17. P. Slepicka, N. Slepicková Kasálková, J. Siegel, Z. Kolská, V. Švorčík, Methods of gold and silver nanoparticles preparation. *Materials* **13**, 1–22 (2020).
18. L. B. Hunt, The true story of Purple of Cassius. The birth of gold-based glass and enamel colours. *Gold Bull.* **9**, 134–139 (1976).
19. D. Shaming, H. Remita, Nanotechnology: From the ancient time to nowadays. *Found. Chem.* **17**, 187–205 (2015).
20. C. Louis, Gold nanoparticles in the past: Before the nanotechnology era, in *Gold Nanoparticles for Physics, Chemistry and Biology* (World Scientific Publishing, ed. 2, 2017), pp. 1–28.
21. F. Wagner, S. Haslbeck, L. Stievano, S. Calogero, Q. A. Pankhurst, K. P. Martinek, Before striking gold in gold-ruby glass. *Nature* **407**, 691–692 (2000).
22. C. M. Cobley, Y. Xia, Gold and nanotechnology. *Elements* **5**, 309–313 (2009).
23. F. J. Heiligtag, M. Niederberger, The fascinating world of nanoparticle research. *Mater. Today* **16**, 262–271 (2013).
24. X. Xu, M. Stevens, M. B. Cortie, In situ precipitation of Gold nanoparticles onto glass for potential architectural applications. *Chem. Mater.* **16**, 2259–2266 (2004).
25. L. Selwym, How to test gold and tin. Canadian Conservation Institute (CCI). Notes 17/6. 19 June 2019; https://www.canada.ca/en/conservation-institute/services/conservation-preservation-publications/canadian-conservation-institute-notes/test-gold-tin.html.
26. C. Chiavari, E. Bernardi, A. Balbo, C. Monticelli, S. Raffo, M. C. Bignozzi, C. Martini, Atmospheric corrosion of fire-gilded bronze: Corrosion and corrosion protection during accelerated ageing tests. *Corros. Sci.* **100**, 435–447 (2015).
27. X. G. Zhang, *Galvanic Corrosion* (John Wiley & Sons Inc., 2011).
28. B. Horemans, C. Cardell, L. Bencs, V. Kontozova-Deutsch, K. De Wael, R. Van Grieken, Evaluation of airborne particles at the Alhambra monument in Granada, Spain. *Microchem. J.* **99**, 429–438 (2011).
29. D. Patrón, H. Lyamani, J. A. Casquero-Vera, G. Titos, G. Mocnik, C. Cardell, L. Alados-Arboledas, F. J. Olmo, Monumental heritage exposure to urban black carbon pollution. *Atmos. Environ.* **170**, 22–32 (2017).

30. S. E. Dunkle, J. R. Craig, J. D. Rimstidt, Romarchite, hydroromarchite and abhurite formed during the corrosion of pewter artifacts from the Queen Anne's Revenge (1718). *Can. Mineral.* **41**, 659–669 (2003).

31. B. Liu, Y. Liu, Study on mechanism of differential concentration corrosion. *Sci. Rep.* **10**, 19236 (2020).

32. M. R. Pinnel, Diffusion-related behaviour of gold in thin film systems. *Gold Bull.* **12**, 62–71 (1979).

33. F. Colin, P. Vieillard, Behavior of gold in the lateritic equatorial environment: Weathering and surface dispersion of residual gold particles, at Dondo Mobi, Gabon. *Appl. Geochem.* **6**, 279–290 (1991).

34. H. Ha, L. Payer, The effect of silver chloride formation on the kinetics of silver dissolution in chloride solution. *Electrochem. Acta* **56**, 2781–2791 (2011).

35. P. Børgesen, M. A. Korhonen, C. Y. Li, Stress and current induced voiding in passivated metal lines. *Thin Solid Films* **220**, 8–13 (1992).

36. R. M. Hough, C. R. M. Butt, J. Fischer-Bühner, The crystallography, metallography and composition of gold. *Elements* **5**, 297–302 (2009).

37. A. J. Forty, Corrosion micromorphology of noble metal alloys and depletion gilding. *Nature* **282**, 597–598 (1979).

38. N. Badwe, X. Chen, D. K. Schreiber, M. J. Olszta, N. R. Overman, E. K. Karasz, A. Y. Tse, S. M. Bruemmer, K. Sieradzki, Decoupling the role of stress and corrosion in the intergranular cracking of noble-metal alloys. *Nat. Mater.* **17**, 887–893 (2018).

39. S. Cherevko, A. A. Topalov, A. R. Zeradjanin, I. Katsounaros, K. J. J. Mayrhofer, Gold dissolution: Towards understanding of noble metal corrosion. *RSC Adv.* **3**, 16516–16527 (2013).

40. P. F. M. Oliveira, A. A. L. Michalchuk, J. Marquardt, T. Feiler, C. Prinz, R. M. Torresi, P. H. C. Camargo, F. Emmerling, Investigating the role of reducing agents on mechanosynthesis of Au nanoparticles. *CrstEngComm* **22**, 6261–6267 (2020).

41. G. Kerr, D. Craw, D. Trumm, J. Pope, Authigenic realgar and gold in dynamic redox gradients developed on historic mine wastes, New Zealand. *Appl. Geochem.* **97**, 123–133 (2018).

42. S. Mohammadnejad, J. Provis, J. S. J. Van Deventer, Reduction of gold(III) chloride to gold(0) on silicate surfaces. *Int. J. Min. Process.* **389**, 252–259 (2013).

43. S. R. King, J. Massicot, A. M. McDonagh, A straightforward route to tetrachloroauric acid from gold metal and molecular chlorine for nanoparticle synthesis. *Metals* **5**, 1454–1461 (2015).

44. R. Tarozaite, R. Juškėnas, M. Kurtinatiene, A. Jagminiene, A. Vaskelis, Gold colloids obtained by Au(III) reduction with Sn(II): Preparation and characterization. *Chem* **17**, 1–6 (2006).

45. H. Hanlie, T. Liyun, Deposition of gold on kaolinite surfaces from $AuCl_4^-$ solution. *Geochem. Int.* **44**, 1246–1249 (2006).

46. A. F. Williams-Jones, R. J. Bowell, A. A. Migdisov, Gold in solution. *Elements* **5**, 281–287 (2009).

# ScienceAdvances

## Natural corrosion-induced gold nanoparticles yield purple color of Alhambra palaces decoration

Carolina Cardell and Isabel Guerra

**View the article online**
https://www.science.org/doi/10.1126/sciadv.abn2541
**Permissions**
https://www.science.org/help/reprints-and-permissions

Use of this article is subject to the Terms of service